Enhancement of Inverse Magnetostrictive Effect through Stress Concentration for a Notch-Introduced FeCo Alloy

doi: 10.1002/adem.201800811

ADVANCED ENGINEERING MATERIALS
www.aem-journal.com

Enhancement of Inverse Magnetostrictive Effect through Stress Concentration for a Notch-Introduced FeCo Alloy

Zhenjun Q1 Yang, Hiroki Kurita, Hiroki Takeuchi, Kenichi Katabira, and Fumio Narita*

The authors investigate the magnetic flux leakage for a class of magnetostrictive FeCo alloys with a notch undergoing compression and impact with respect to energy harvesting. The magnetic flux leakage plays a crucial role in the practical energy transition in terms of the features for energy harvesting. Therefore, the corresponding situations are systematically studied by combining finite element analysis (FEA) with practical experiments. The FeCo alloys are categorized into three groups with different three-dimensional notch shapes, and the depths of the notches are 0, 0.5, and 1 mm, respectively. The parameters in both the simulations and practical tests are completely consistent. The results of compression test carried out with a stepwise-increasing stress from 0 to 100 MPa reveal that the variations of magnetic induced flux increase with the increasing depth of the notches. The following FEA herein provides a feasible interpretation that the stress concentration around the notch is largely responsible for the notch-induced enhancement. The findings of the impacting experiments simultaneously exhibit an analogous tendency that the output power is proportional to the depth of notch. Furthermore, the stress rate has no obvious effect on the output electricity. The maximum magnitude of the improvement for the output power increases by almost 400% comparing the specimens with notches of 0 and 1 mm. This study indicates a promising feasibility to achieve vibration-energy harvesting from various irregular components.

1. Introduction

Applications of novel energy harvesting materials have been gaining noteworthy consideration in self-power micromechanical systems, the internet of things (IoT), and so on. Harvesting of wasted energy (vibration, thermal energy, etc.) plays an increasing role in supporting milli-scale commercial nodes with power ranging from 0.1 to 1000 μW.[1] Currently, high-performance harvesting materials, like the classes of piezoelectric ceramics/polymers and magnetostrictive alloys, have been employed in various power-generating devices.[2–4] However, with the rapid rate of IoT innovation, the further requirements for high-power-generating components are an imminent challenge.

The feasibility of using magnetostrictive materials for power-generating components has been practically demonstrated,[5] especially for the applications of vibration-energy harvesting in terms of their inverse magnetostrictive properties.[6] In the current decade, there are two dominant magnetostrictive materials known as Terfenol-D and Galfenol that have been widely studied. The Terfenol-D is often of sizable magnetostriction and low magnetic anisotropy, and it has therefore been considered as a promising energy harvesting components at the beginning.[7] However, natural demerits such as high brittleness and low resistance to cyclic loading impede its further application[8] especially as a vibration energy harvesting component.[9,10] On the other hand, although Galfenol alloy has some metallic properties, the processing costs (high-cost production, sophisticated processing, etc.) are also considered as a vital problem with respect to application in energy harvesting devices. Some researchers have fabricated a series of composites to resolve these problems at the expense of the reduction of magnetostrictive properties. Nevertheless, the final results demonstrated that there is only a limited improvement for energy harvesting effectiveness.[11,12]

A class of iron–cobalt alloys (FeCo) is known for its good magnetostrictive properties. This kind of material is therefore capable of being applied in energy harvesting equipments on the basis of its cost-effective and easily-processing merits in comparison to Terfenol-D and Galfenol. A nominal composition of this class of alloys can be denoted as $Fe_{1-x}Co_x$ ($x = 50$–90 at %) Q3.[13] In recent year, forging and certain mechanical treatments were used to fabricate the FeCo-related composite and the experimental performance for the output electricity was reported.[14] We have fabricated a new 1–3 composite whereby FeCo wires (a diameter of 1 mm) were embedded into a polymer matrix,[15] and the results revealed that the output voltage of this composite is clearly proportional to compressive stress. Moreover, the maximum voltage of the aforementioned 1–3 composite was about two times than that of Galfenol. The relevant mechanism is closely associated with the effect of tensile prestress stemming from the curing process of the

F. Narita, Z. J. Yang, H. Kurita, H. Takeuchi, K. Katabira Q2
Department of Materials Processing
Graduate School of Engineering
Tohoku University
Sendai 980-8579, Japan
E-mail: narita@material.tohoku.ac.jp

The ORCID identification number(s) for the author(s) of this article can be found under https://doi.org/10.1002/adem.201800811.

DOI: 10.1002/adem.201800811

polymer matrix, and this specific characteristic therefore has the benefit of speeding up the variation of magnetic induced flux. Here, for a magnetostrictive material that has been magnetized, applied stress is easily able to change the direction of magnetic field as a result of the rotation of domain and/or the movement of domain wall, and furthermore, it then leads to a variation for magnetic induced flux. Additionally, a further experiment[16] showed the correlation between the diameter and stress-induced output voltage by altering the diameter of the fiber from 1 to 0.2 mm. More recently, we have fabricated magnetostrictive polymer composites, in which FeCo fibers were woven into polyester fabric, and discussed their sensor performance.[17] We also have proposed a magnetostrictive clad steel plate for harvesting vibration energy.[18] It comprised a cold-rolled FeCo alloy and cold-rolled steel joined together by thermal diffusion bonding, and the results indicated that the clad steel plate construct exhibits high voltage and power output compared to a single-plate construct. It is not difficult to realize that this class of FeCo have a promising capacity of serving as high-performance component for vibration energy harvesting.

The magnetostrictive properties of materials has a significant effect on energy transmission. According to some current researches on FeCo-related magnetostrictive energy harvesting devices, the magnetic flux variation in response to the applied force plays a vital role in exciting the output electricity. Equivalently, a method to magnify the stress through a desirable shape design can be another way to further enhance the harvesting energy. The purpose of this study is to discuss the effect of the notch on the inverse magnetostrictive performance of FeCo alloy and to analyze the variations of magnetic induced flux in the FeCo alloy. Furthermore, this study explores a feasibility of harvesting vibration energy for the irregular component.

2. Experimental Section

The FeCo alloys were processed into rectangular specimens with length $l = 15$ mm, width $w = 5$ mm, and thickness $h = 3$ mm. A notch was introduced, with depths of $d = 0$, 0.5, and 1 mm and a width of $c = 5$ mm. The dimensional details are shown in **Figure 1**a. A rectangular Cartesian coordinate system O-xyz is used and the origin of the coordinate system coincides with the center of the upper surface (see Figure 1b). Briefly, the practical experiments were classified into two parts of compression and impact, shown in **Figure 2**. The compressive tests were performed as shown in **Figure 3**a. The compressive stresses varied from 0 to 100 MPa by totally 15 steps. Here, the nominal stress σ_0 was calculated by dividing the static compressive load P_0 by the cross-section area $A = wh$ of specimen without notch. The bias magnetic field B_{0z} is 0 and 350 mT, respectively. The cross-section of the outside magnet is completely consistent with that of specimen. A Tesla meter was used to measure the real-time variation of magnetic induced flux ($\triangle B_z$) at the point near $x = w - d$, $y = 0$, and $z = 0$ resulting from the applied compressive load (the detailed position of the probe has been shown in Figure 3a).

After that, the impact tests were performed as shown in Figure 3b. The specimen was enclosed by the coil wounds at an inductance of 12.6 mH and a length of 15 mm. Further, an impulsive hammer kit GK-3100 (ONO SOKKI CO. LTD., Japan) was used to impact this device. The load P was increased from 0 to the maximum load P_{max}. A versatile oscilloscope (GDS-1062A) connected to the harvesting setup (coil wounds) and hammer with a sensor was used to measure the real-time output power and applied stress $\sigma = P/A$ (applied maximum stress $\sigma_{max} = P_{max}/A$) simultaneously. An electric circuit at a loading resistance of 10 kΩ, connected to the harvesting coil wounds, is used to estimate the power-generation performance of this class of FeCo alloys. Note that the bias magnetic field (B_{0z}) held a consistent value of 350 mT.

3. Analysis

In order to comprehensively understand the mechanism of the variation of magnetic induced flux for the FeCo specimen with a notch, the FEA was performed to provide insights into the reasons for the stress-induced distinctions of magnetization. The equilibrium equations are given by

$$\sigma_{jij} = 0 \tag{1}$$

$$e_{ijk} H_{k,j} = 0,\ B_{i,i} = 0 \tag{2}$$

where σ_{ij}, H_i, and B_i are the components of the stress tensor, magnetic field intensity vector, and magnetic flux vector, respectively, e_{ijk} is the permutation symbol, and a comma denotes partial differentiation with respect to the coordinates

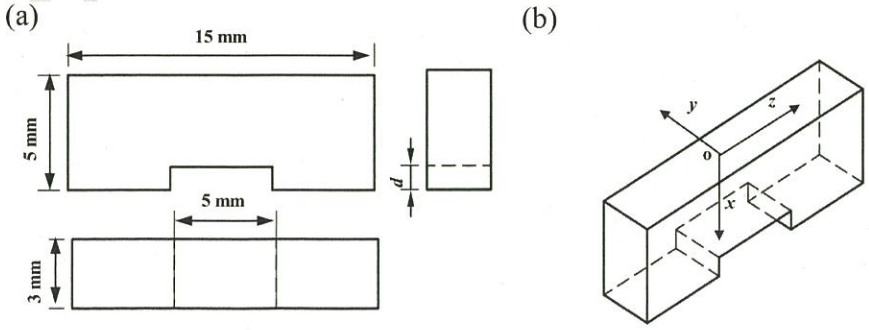

Figure 1. Schematics for a) the section and b) the perspective drawing of the experimental specimen with a notch.

$x_i (i = 1, 2, 3)$. We have employed Cartesian tensor notation and the summation convention over repeated tensor indices. Constitutive relations can be given by

$$\varepsilon_{ij} = s^H_{ijkl}\sigma_{kl} + d'_{kij}H_k \tag{3}$$

$$B_i = d'_{ikl}\sigma_{kl} + \mu_{ik}H_k \tag{4}$$

where ε_{ij} is the component of the strain tensor, and s^H_{ijkl}, d'_{kij}, and μ_{ik} are the constant magnetic field elastic compliance, magnetoelastic constant, and magnetic permeability, which satisfy the following symmetry relations:

$$s^H_{ijkl} = s^H_{jikl} = s^H_{ijlk} = s^H_{klij},\ d'_{kij} = d'_{kji}, \mu_{ij} = \mu_{ji} \tag{5}$$

The strain component is given by

$$\varepsilon_{ij} = \frac{1}{2}(u_{j,i} + u_{i,j}) \tag{6}$$

where u_i is the component of the displacement vector. The component of the magnetic field intensity vector is

$$H_i = \varphi_{,i} \tag{7}$$

where φ is the magnetic potential. The constitutive Equation (3) and (4) are given by

$$\begin{Bmatrix} \varepsilon_{11} \\ \varepsilon_{22} \\ \varepsilon_{33} \\ 2\varepsilon_{23} \\ 2\varepsilon_{31} \\ 2\varepsilon_{12} \end{Bmatrix} = \begin{bmatrix} s^H_{11} & s^H_{12} & s^H_{13} & 0 & 0 & 0 \\ s^H_{12} & s^H_{11} & s^H_{13} & 0 & 0 & 0 \\ s^H_{13} & s^H_{13} & s^H_{33} & 0 & 0 & 0 \\ 0 & 0 & 0 & s^H_{44} & 0 & 0 \\ 0 & 0 & 0 & 0 & s^H_{44} & 0 \\ 0 & 0 & 0 & 0 & 0 & s^H_{66} \end{bmatrix} \begin{Bmatrix} \sigma_{11} \\ \sigma_{22} \\ \sigma_{33} \\ \sigma_{23} \\ \sigma_{31} \\ \sigma_{12} \end{Bmatrix} + \begin{bmatrix} 0 & 0 & d'_{31} \\ 0 & 0 & d'_{31} \\ 0 & 0 & d'_{33} \\ 0 & d'_{15} & 0 \\ d'_{15} & 0 & 0 \\ 0 & 0 & 0 \end{bmatrix} \begin{Bmatrix} H_1 \\ H_2 \\ H_3 \end{Bmatrix} \tag{8}$$

$$\begin{Bmatrix} B_1 \\ B_2 \\ B_3 \end{Bmatrix} = \begin{bmatrix} 0 & 0 & 0 & 0 & d'_{15} & 0 \\ 0 & 0 & 0 & d'_{15} & 0 & 0 \\ d'_{31} & d'_{31} & d'_{33} & 0 & 0 & 0 \end{bmatrix} \begin{Bmatrix} \sigma_{11} \\ \sigma_{22} \\ \sigma_{33} \\ \sigma_{23} \\ \sigma_{31} \\ \sigma_{12} \end{Bmatrix} + \begin{bmatrix} \mu_{11} & 0 & 0 \\ 0 & \mu_{11} & 0 \\ 0 & 0 & \mu_{33} \end{bmatrix} \begin{Bmatrix} H_1 \\ H_2 \\ H_3 \end{Bmatrix} \tag{9}$$

where

$$\sigma_{23} = \sigma_{32}, \sigma_{31} = \sigma_{13},\ \sigma_{12} = \sigma_{21} \tag{10}$$

$$\varepsilon_{23} = \varepsilon_{32}, \varepsilon_{31} = \varepsilon_{13},\ \varepsilon_{12} = \varepsilon_{21} \tag{11}$$

$$\begin{aligned} s^H_{11} &= s^H_{1111} = s^H_{2222}, s^H_{12} = s^H_{1122}, s^H_{13} = s^H_{1133} = s^H_{2233}, s^H_{33} \\ &= s^H_{3333}, s^H_{44} = 4s^H_{2323} = 4s^H_{3131}, s^H_{66} = 4s^H_{1212} = 2\left(s^H_{11} - s^H_{12}\right) \end{aligned} \tag{12}$$

$$d'_{15} = 2d'_{131} = 2d'_{223}, d'_{31} = d'_{311} = d'_{322}, d'_{33} = d'_{33} \tag{13}$$

Here, a three-dimensional finite element model is created in order to calculate the magnetic flux and stress distributions for the FeCo alloys with and without a notch. **Figure 4** shows the finite element mesh and boundary conditions. Let the coordinate axes $x = x_1$ and $y = x_2$ be chosen such that the $z = x_3$ axis coincides with the easy axis of the magnetization. In the experiments, a bias magnetic field is along the length direction (easy axis), and the longitudinal (33) magnetostrictive deformation mode is dominant. Hence, the constants d'_{15}, d'_{31}, and d'_{33} are

$$\begin{aligned} d'_{15} &= d^m_{15} \\ d'_{31} &= d^m_{31} \\ d'_{33} &= d^m_{33} + m_{33}H_3 \end{aligned} \tag{14}$$

where d^m_{15}, d^m_{31}, and d^m_{33} are the piezo-magnetic constants, and m_{33} is the second-order magnetoelastic constant. Finite element calculations were carried out to obtain the variations of magnetic induced flux and stress distributions. The basic equations for the magnetostrictive materials are mathematically equivalent to those for piezoelectric materials. So, the commercial package ANSYS with coupled-field solid, acoustic fluid, and infinite acoustic elements was used in the simulation. In the analysis, the bias magnetic field B_{0z} and compressive load P in the z-direction were applied to the FeCo alloys for some notch sizes.

The simulating parameters (bias magnetic field, load, etc.) were employed as almost same as those of the practical experiments. The relevant properties of FeCo alloys associated with the calculation for FEA are listed in **Table 1**.[17] The parameter of m_{33} is $0.0123 \times 10^{-12}\,\mathrm{m^2\ A^{-2}}$. Air density of $1.2\,\mathrm{kg\,m^{-3}}$ is assumed in calculating the magnetic field distribution in the air. The sizes of the air are assumed to be $75 \times 15 \times 25\ \mathrm{mm^3}$. Furthermore, the magnetic permeability μ_0 of free space is $1.26 \times 10^{-6}\ \mathrm{H\ m^{-1}}$.

4. Results

It was investigated that the variation of magnetic induced flux for the FeCo alloys with notches of differing depths under the compressive stresses. **Figure 5** presents the results of practical experiments which show the variation of magnetic induced flux ΔB_z at $x = w - d$, $y = 0$, and $z = 0$ with the applied stress σ_0. The obtained results from the FEA were also plotted. The variation of magnetic induced flux for these two specimens with different

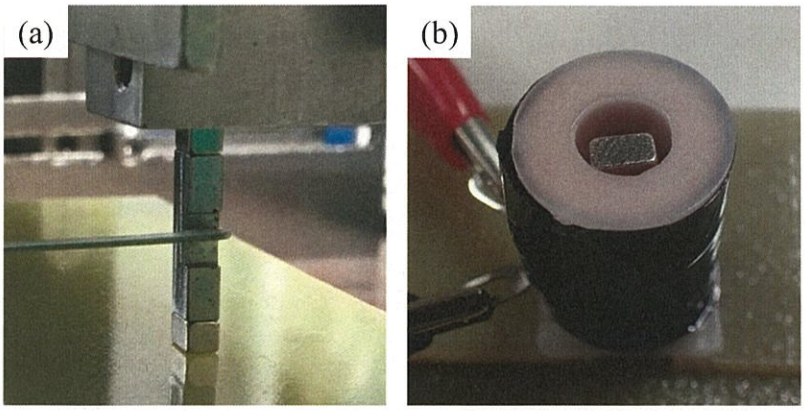

Figure 2. Physical assemblies for a) the compression and b) the impacting experiment.

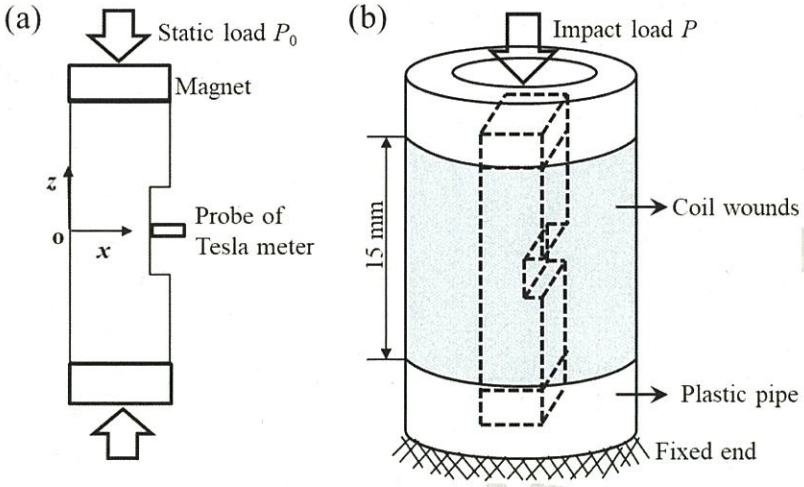

Figure 3. Schematics for a) the compression and b) impacting experiment.

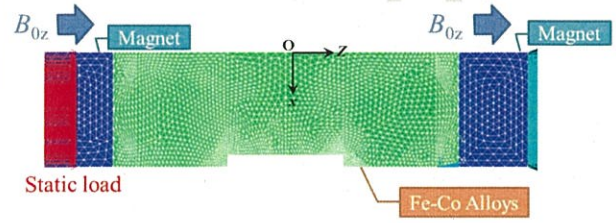

Figure 4. Schematic of mesh and boundary conditions for the FEA.

notches were certainly proportional to the applied stresses. The variation of magnetic induced flux showed a dramatically increasing tendency with increase of the depth of notch. In addition, the varied tendencies stemming from the results of FEA were almost consistent with that of the aforementioned experiment on the whole. Considering the necessity for the bias magnetic field, the corresponding effects of the distinct magnetic fields were also investigated. As concerns the comparison of the variation of magnetic induced flux shown in **Figure 6**, it is obvious that the powerful bias magnetic field is easily capable of magnetizing the materials, in this case, the perturbation of the applied stress on the variation of magnetic induced flux was substantially magnified.

The stress distribution around a notch are shown in **Figure 7**. It was also verified that the distribution of stress has distinct features around the notch in comparison to other areas, where different colors were used to denote the localized magnitude for the stress distribution. On the other hand, as mentioned above, an irregular shape was capable of giving rise to a localized stress concentration. In order to predict the tendency and optimize the parameters of the notch-liked irregular shape, FEA has been conducted to give a feasible prediction. **Figure** 8a and b shows the variations of magnetic induced flux ΔB_z at $x = w - d$, $y = 0$, and $z = 0$ versus notch depth d and notch width c, respectively. Furthermore, the variations of energy density for the samples with notches of 0.5 and 1 mm were also simulated under loadings ranging from 0 to 100 MPa. Figure 8c shows the values are 13.05 and 25.44 J mm^{-3}, respectively. The comparison indicates a clear coherency of the prediction and practical measurement. That is, the variation of magnetic induced flux is proportional to the depth of the notch (d) but decreases with increase of the width of the notch (c).

The impacting experiment was performed to explore the relevance between the impact-induced output power and depths of notch. **Figure 9** shows the measured output power versus stress-rate $d\sigma/dt$ (where t is time) and the maximum stress σ_{max}. According to the foregoing findings of the compression, the reason responsible for the change of the output power is nearly

Table 1. Material properties of FeCo alloys.

Elastic compliance [$\times 10^{-12}$ m^2 N^{-1}]						Piezomagnetic constant [$\times 10^{-12}$ m^2 A^{-1}]			Permeability [$\times 10^{-6}$ H m^{-1}]	
S_{11}^H	S_{33}^H	S_{44}^H	S_{66}^H	S_{12}^H	S_{13}^H	d_{31}	d_{33}	d_{15}	μ_{11}	μ_{33}
5.5	5.5	14.3	14.3	−1.65	−1.65	−60.3	125	318	37.7	37.7

COLOR

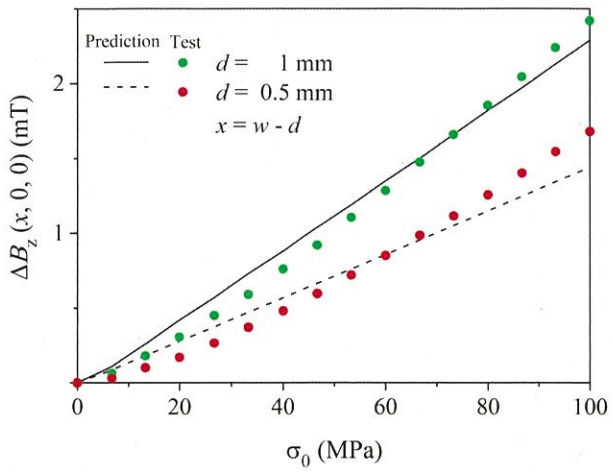

Figure 5. Comparison of the magnetic flux changes for the FeCo alloys with different notches between practical experiment and FEA.

consistent with that of the compression, namely, the output powers show an upward tendency with the increasing depths of notches. This hypothesis has been validated and is shown in Figure 9. Furthermore, the notch-induced maximum enhancement soars by almost 400%, seen from the comparison between the output power of the specimen with a notch of 1 mm and that of 0 mm. Through this diagram, it is not difficult to understand that the magnitude of stress has an effect on the output power. However, due to the existence of the notch, the increase of power generation was also obvious. Additionally, it seems that the stress rate had no inherent effect on the change of output power.

5. Discussion

Here, the correlation between notch and power generation has been studied under the situations of compression and impacting, respectively. The results revealed that there was a close consistency, that is, the specimen with a deep notch apparently contributed to the improvement of power-generating performance. According to the FEA, the findings provide some insights into the understanding of the mechanism in response to the stress-concentration enhancement for power generation. Generally, the stress-induced perturbation for the variation of magnetic induced flux is highly proportional to the applied compressive stress according to the mechanism of the inverse magnetostrictive effect. Hence, it is predictable that the stress concentration is the main reason for the speed-up variation of magnetic induced flux, which then further causes the increase of power generation. Furthermore, the considerable green area symbolizing the stress concentration is the predominant segment around the notch. In one sense, this distributional feature has substantiated that the notch-induced stress concentration is closely related to the improvement for power generation. However, this is slightly inadequate to interpret the detailed procedure when the stress varied from 0 to 100 MPa. When observing the enlarged area around the notch carefully, in addition to the stress-concentration area, the existence of a stress-releasing area (the value of stress is somewhat lower than the average of the whole specimen) indicates that the corresponding perturbation in each part stemming from the loading is of inconsistent magnitude, even appearing the opposite variation for magnetic induced flux. In particular, the neighboring domain has been magnetized in reverse, as shown by the red and yellow parts in Figure 7b. As a consequence, there may be a slight fluctuation for the variation of magnetic induced flux during the entire procedure. Further, it is imperative to analyze the specific and dynamic stress change within the specimen in future experiments, especially around the notch.

COLOR

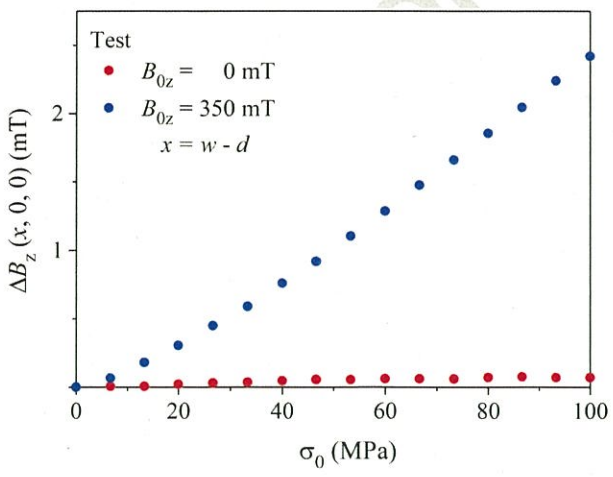

Figure 6. Comparison of the magnetic flux changes for the FeCo alloys with a notch of 1 mm depth under differing bias magnetic fields of 0 and 350 mT.

COLOR

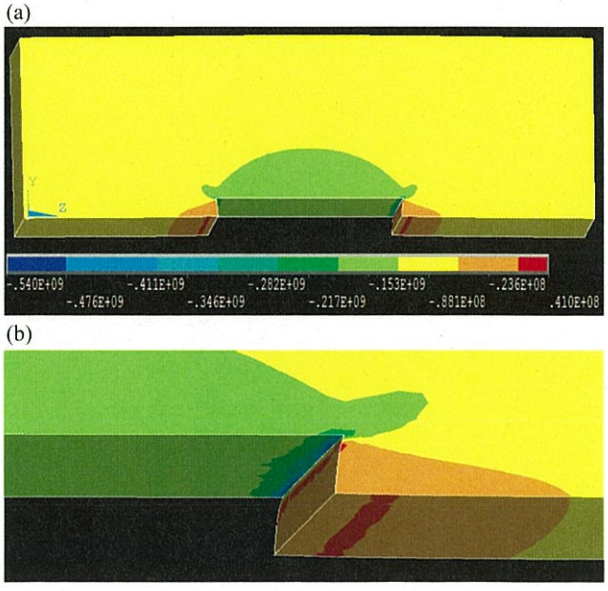

Figure 7. Simulations for a) the distribution of stress within the whole specimen under a compressive loading of 100 MPa and b) the enlarged features around the notch.

COLOR

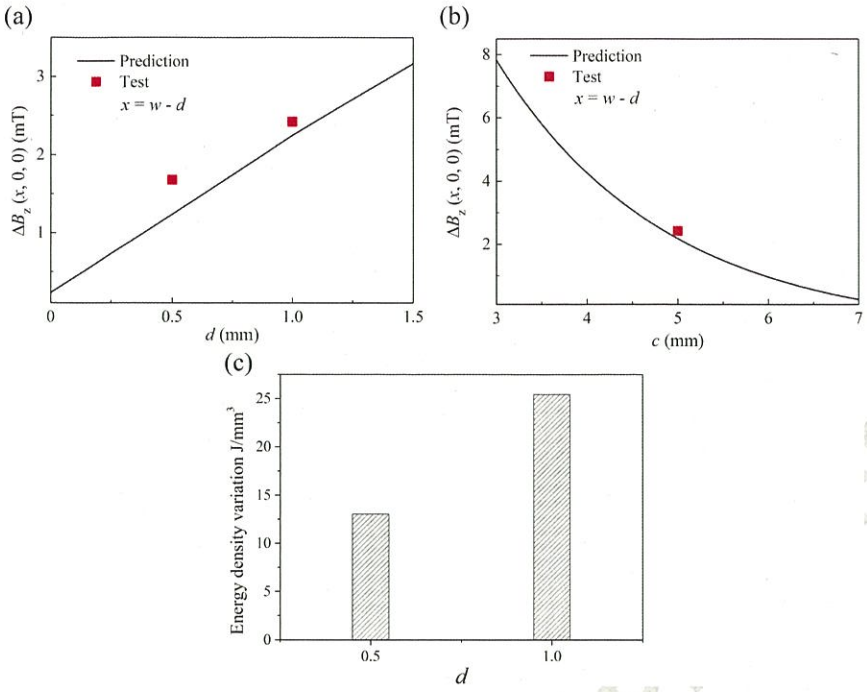

Figure 8. Comparison of the magnetic flux changes for prediction and measurement with a) differing depths of notches at a constant width of 5 mm and b) differing widths of notches at a constant depth of 1 mm; c) variations of the energy density for differing depths of notches under loadings ranging from 0 to 100 MPa.

COLOR

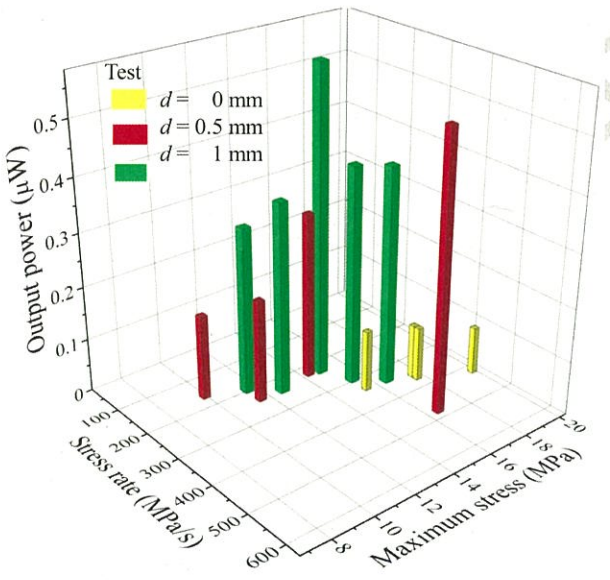

Figure 9. Diagram of the output power for the specimens with different notches.

6. Conclusion

This article has experimentally and theoretically analyzed the variation of magnetic induced flux and output power generation for a class of FeCo alloys in response to notches with differing depths. In conclusion, the findings have ultimately demonstrated that the stress concentration around the notch is mainly responsible for conspicuous increases in the variation of magnetic induced change and output power generation. Furthermore, this study has also explored a promising feasibility to achieve high-performance energy harvesting through the irregular design of the notch shape.

Conflict of Interest

The authors declare no conflict of interest.

Keywords

electromagneto-mechanics, energy harvesting, iron-cobalt alloys, notch, simulation & testing

Received: July 26, 2018
Revised: September 14, 2018
Published online:

[1] S. Balpande, R. S. Pande, R. M. Patrikar, *Sens. Actuators A-Phys.* **2016**, *251*, 134.
[2] Z. Lin, J. Chen, X. Li, J. Li, J. Liu, Q. Awais, J. Yang, *Appl. Phys. Lett.* **2016**, *109*, 253903.
[3] F. Narita, M. Fox, *Adv. Eng. Mater.* **2018**, *20*, 1700743.
[4] Z. Wang, S. Abe, F. Narita, *Res. Dev. Mater. Sci.* **2018**, *5*, 000607.
[5] A. E. Clark, B. F. Desavage, R. Bozorth, *Phys. Rev.* **1965**, *138*, A216.

[6] A. Adly, D. Davino, A. Giustiniani, C. Visone, *J. Appl. Phys.* **2010**, *107*, 09 A935.
[7] K. Mori, T. Horibe, S. Ishikawa, Y. Shindo, F. Narita, *Smart Mater. Struct.* **2015**, *24*, 125032.
[8] M. Colussi, F. Berto, K. Mori, F. Narita, *Adv. Eng. Mater.* **2016**, *18*, 2063.
[9] N. Adelsberg, Y. Weber, A. Yoffe, D. Shilo, *Smart Mater. Struct.* **2017**, *26*, 065013.
[10] M. Nascimento, G. Chesini, J. M. Baptista, C. M. B. Cordeiro, P. A. S. Jorge, *IEEE Sens. J.* **2017**, *17*, 6615.
[11] M. Y. Alnassar, Y. P. Ivanov, J. Kosel, *Adv. Electron. Mater.* **2016**, *2*, 1600081.
[12] N. L. Raveendran, R. Pandian, S. Murugesan, K. Asokan, R. T. R. Kumar, *J. Alloys Compd.* **2017**, *704*, 420.
[13] H. Cheng, Y. G. Wang, D. Xie, *Mater. Lett.* **2015**, *143*, 273.
[14] S. Yamaura, T. Nakajima, T. Satoh, T. Ebata, Y. Furuya, *Mater. Sci. Eng. B-Adv.* **2015**, *193*, 121.
[15] F. Narita, *Adv. Eng. Mater.* **2017**, *19*, 1600586.
[16] F. Narita, K. Katabira, *Mater. Trans.* **2017**, *58*, 302.
[17] K. Katabira, Y. Yoshida, A. Masuda, A. Watanabe, F. Narita, *Materials* **2018**, *11*, 406.
[18] Z. Yang, K. Nakajima, R. Onodera, T. Tayama, D. Chiba, F. Narita, *Appl. Phys. Lett.* **2018**, *112*, 073902.

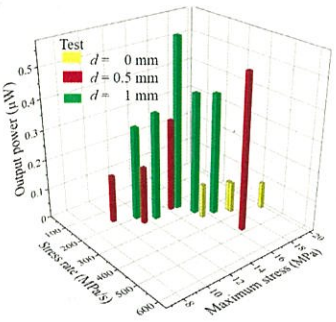

The effects of a notch on vibration energy harvesting for a magnetostrictive material is proposed. The relationship between the notch and energy conversion is systematically examined through practical experiment and finite element analysis. The results indicate that the output power is proportional to the depth of notch as a result of localized stress concentration.